Investigation of aluminum nitrate as a set retarder of magnesium potassium phosphate cement: Mechanisms involved in diluted suspension

Céline Cau Dit Coumes, Angélique Rousselet, Biwan Xu, Cyrille Albert Mercier, sandrine Gauffinet

▶ **To cite this version:**

Céline Cau Dit Coumes, Angélique Rousselet, Biwan Xu, Cyrille Albert Mercier, sandrine Gauffinet. Investigation of aluminum nitrate as a set retarder of magnesium potassium phosphate cement: Mechanisms involved in diluted suspension. Cement and Concrete Research, 2021, 150, pp.106608. 10.1016/j.cemconres.2021.106608 . hal-04280341

HAL Id: hal-04280341
https://hal.science/hal-04280341

Submitted on 10 Nov 2023

HAL is a multi-disciplinary open access archive for the deposit and dissemination of scientific research documents, whether they are published or not. The documents may come from teaching and research institutions in France or abroad, or from public or private research centers.

L'archive ouverte pluridisciplinaire **HAL**, est destinée au dépôt et à la diffusion de documents scientifiques de niveau recherche, publiés ou non, émanant des établissements d'enseignement et de recherche français ou étrangers, des laboratoires publics ou privés.

Cement and Concrete Research 150 (2021) 106608

Contents lists available at ScienceDirect

Cement and Concrete Research

journal homepage: www.elsevier.com/locate/cemconres

Investigation of aluminum nitrate as a set retarder of magnesium potassium phosphate cement: Mechanisms involved in diluted suspension

Céline Cau Dit Coumes [a,*], Angélique Rousselet [b], Biwan Xu [a], Cyrille Albert Mercier [c], Sandrine Gauffinet [b]

[a] CEA, DES, ISEC, DE2D, Univ Montpellier, Marcoule, France
[b] UMR6303 CNRS Université Bourgogne/Franche-Comté, Faculté des Sciences Mirande, 9 Avenue, Alain Savary, BP 47870, 21078 Dijon cedex, France
[c] Laboratoire des Matériaux Céramiques et Procédés Associés (LMCPA), Université de Valenciennes et du Hainaut-Cambrésis, 59600 Maubeuge, France

ARTICLE INFO

Keywords:
Magnesium potassium phosphate cement
Aluminum nitrate
Hydration
Thermodynamic modelling

ABSTRACT

In this study, the influence of aluminum nitrate on the hydration process of magnesium potassium phosphate (MKP) cement was investigated experimentally and through thermodynamic modelling using diluted systems with Mg/PO_4 molar ratio and water-to-cement ratio of 1 and 100 respectively. Three processes contributed to retard cement hydration: the acidic nature of aluminum nitrate which reduced the initial pH of the solution by two units, the early precipitation of a taranakite-like amorphous potassium aluminophosphate, which reduced the aqueous phosphate and potassium concentrations, and a salt effect due to the presence of soluble nitrate. Precipitation of potassium-containing magnesium phosphate hydrates, like $Mg_2KH(PO_4)_2{\cdot}15H_2O$ and K-struvite, was prohibited, whereas precipitation of newberyite and cattiite was delayed. Furthermore, the modelled phase development with ongoing cement hydration agreed rather well with the experimental findings.

1. Introduction

Magnesium potassium phosphate (MKP) cements are an alternative to Portland cement for niche applications. They harden through the so-called 'acid-base' reaction between hard-burnt or dead-burnt magnesia and monopotassium phosphate (KH_2PO_4), which more precisely is a dissolution-precipitation hydration process. As compared to Portland cement, MKP cements have different advantages, such as fast setting [1–3], high early strength [2–5], low shrinkage [2,3], strong bonding with Portland cement concrete substrates [2,6], low pH [3,7,8], good immobilization of heavy metals [9,10], and good biocompatibility [11,12]. Therefore, they can be used as rapid repair materials for damaged infrastructure [2], as conditioning agents for wastes with heavy metals [9,10], and as potential cementitious binders to stabilize and solidify low-level or intermediate-level radioactive wastes [7,8,13–17]. Recent research also considered their use as bioengineering materials [11,12], bipolar plates for fuel cells [18] and 3D printing materials [19].

The hydration path of MKP cements can be adjusted by using different magnesium-to-phosphate (Mg/PO_4) molar ratios [3,4,20–23] or water-to-cement (w/c) ratios [3,7,8,20,22], by adding chemical admixtures [7,8], e.g. borax or boric acid, and by incorporating mineral additions, e.g. fly ash [14,24], metakaolin [24], and wollastonite [25]. However, the predominant hardening reaction of MKP cements can always be described as:

$$MgO + KH_2PO_4 + 5H_2O \rightarrow MgKPO_4{\cdot}6H_2O\ (K-struvite) + Q_{heat} \quad (1)$$

As shown, K-struvite is the stoichiometric hydrate of MKP cements. Furthermore, the reaction releases significant heat [3,26], which accelerates cement hydration, causes too fast setting, and makes it difficult to use cement in large amounts [1,27]. The ability to control cement hydration is thus quite crucial. In the literature, several methods have been proposed to slow down cement hydration, including *(i)* use of cold water [28], *(ii)* decrease in magnesia reactivity [5], *(iii)* increase in the initial pH of the pore solution by partially replacing KH_2PO_4 with either K_2HPO_4 [29] or $Na_2HPO_4{\cdot}12H_2O$ [30], *(iv)* cement dilution with mineral additions, e.g. fly ash [14,24], metakaolin [24], and wollastonite [25], and *(v)* use of different chemicals, such as sodium tripolyphosphate [27], calcium nitrate [31], sodium sulfate [31], and boron compounds [2,7,14]. Among those proposed chemicals, boric acid and borax are the most popular and de facto standard retarders for MKP cements. In addition, boron compounds have been used as set retarders for other cements, such

* Corresponding author.
E-mail address: celine.cau-dit-coumes@cea.fr (C. Cau Dit Coumes).

https://doi.org/10.1016/j.cemconres.2021.106608
Received 4 January 2021; Received in revised form 2 June 2021; Accepted 15 September 2021
Available online 24 September 2021
0008-8846/© 2021 Elsevier Ltd. All rights reserved.

as Portland cement [32], alkali-activated cement [33] and calcium sulfoaluminate cement [34,35]. However, the retardation mechanisms are somewhat different among those cements, due to their different chemistries. Recent studies [7,8] have unveiled the underlying retardation mechanisms of boric acid in MKP cements at a Mg/PO_4 molar ratio of 1 and w/c ratios of 1 and 100. It has been shown that boric acid slows down the precipitation of the reaction products rather than the dissolution of the cement components. Further, two retardation processes have been evidenced: *(i)* stabilization of cations in the cement pore solution to outbalance the negative charges of borates and polyborates formed at pH above 6, and *(ii)* precipitation of one or several amorphous hydrates containing borate and orthophosphate at a w/c ratio of 1. In general, with addition of boron compounds at concentrations of a few percent with respect to the mass of cement, the setting time of MKP cement-based materials can vary from several to tens of minutes [2,3,5,25,27]. MKP cements are thus mainly used for niche applications [1,27]. Larger contents of boron compounds, e.g. a borax addition level of 10 wt% [5], led to material strength loss, especially at early age. Moreover, boron compounds are now included in the EU candidate list of substances of very high concern for authorization, due to their reproductive toxicity. Therefore, the use of boron compounds is becoming restricted in Europe. All of these elements emphasize the research significance of exploring alternative set retarders to boron compounds, with equal or even better retardation effect and higher safety to humans.

This work was undertaken within a project aiming at developing a cement matrix for the conditioning of reactive metals such as aluminum. For this application, the Mg/PO_4 molar ratio was set to 1, the stoichiometric ratio as shown in reaction (1), to keep the pore solution pH of the hardened matrix within the passivation domain of aluminum [36,37]. In a preliminary study, aluminum nitrate nonahydrate ($Al(NO_3)_3{\cdot}9H_2O$) was tested as a set admixture, in replacement of boric acid or borax. It produced a notable retardation effect, with a final setting time of 8 h for the investigated cement paste, against 1.2 h for the same material without any admixture (see Appendix A for more details). The retardation mechanism of aluminum nitrate was thus further explored. For characterization of fast reacting cement systems, diluted cement suspensions have been frequently used [3,7,8,22,25,38] to extend the different hydration stages and thus make characterizations on solid and aqueous phases easier. However, if the dilution factor is too large, the solution may remain undersaturated with respect to the minerals that would precipitate in pastes, thus modifying the hydration process. Therefore, the study was divided in two parts. Experiments were first carried out on suspensions, and then on pastes. This paper reports the results obtained at high w/c ratio of 100. Cement hydration was investigated using a large panel of techniques: electrical conductimetry, pH measurement and composition analysis by ICP-AES for the aqueous phase, X-Ray diffraction and MAS-NMR (^{31}P, ^{27}Al) for the solid phase. The experimental results were then compared to simulations performed with a geochemical speciation code and a thermodynamic database enriched with relevant phosphate minerals and aqueous species.

2. Materials and methods

2.1. Materials

The starting raw materials used to prepare the MKP cement suspension included a hard-burnt magnesia, KH_2PO_4 and deionized water. The hard-burnt magnesia (MAGCHEM 10 CR from M.A.F. Magnesite BV) had a purity of 98.3% (Table 1), a specific surface area of 0.9 m^2/g and a mean particle size (d_{50}) of 18.9 μm. The adopted KH_2PO_4 (supplied by VWR) had a purity >98% and a mean particle size (d_{50}) of 365 μm.

Table 1
Magnesia chemical composition, wt%.

MgO	CaO	SiO_2	Fe_2O_3	Al_2O_3	SO_3	Cl	L.O.I.[a]
98.3	0.9	0.4	0.2	0.1	0.01	0.01	0.25

[a] Loss on ignition.

Table 2 shows the mix designs of the investigated cement suspensions. All the cement suspensions had the same Mg/PO_4 molar ratio of 1, the same high w/c ratio of 100, and a same concentration of 20 mmol/L for boric acid and aluminum nitrate. The crystallization water of aluminum nitrate nonahydrate was taken into account in the calculation of the w/c ratio.

The formulation parameters were selected for the following reasons:

- As explained in introduction, setting the Mg/PO_4 to 1 was beneficial to mitigate the corrosion of metallic aluminum encapsulated in the MKP matrix. Moreover, there is an issue regarding the long-term volume stability of a MKP material containing residual MgO in the humid environment of a repository since it is well-known that hydration of MgO into $Mg(OH)_2$ is accompanied by a significant (118%) volume increase [39].
- The w/c ratio of 100 was the same as that of a previous work investigating the retarding effect of boric acid [7]. It resulted from a compromise making it possible to sample a reasonable number of aliquots for analysis without changing significantly the water-to-cement ratio, to increase the duration of the different stages of hydration, and to precipitate cement hydrates.
- The $B(OH)_3$ concentration of 20 mmol/L corresponded to a typical boric acid-to-cement weight ratio (1.24%) and was shown to retard significantly the hydration process of MKP cement [7].

2.2. Methods

2.2.1. Electrical conductivity and pH measurement

Electrical conductivity of the cement suspensions was measured in real-time using a Multicad CDM 210 conductimeter. According to the mix designs in Table 2, the setting admixture and KH_2PO_4 powder were firstly dissolved in deionized water that was stored in a vessel at a temperature regulated at 25 °C. Afterwards, magnesia was added to the solution, along with a continuous mixing using a magnetic stirrer and a data-recording at time steps of 1 min. The vessel containing the prepared suspension was sealed in order to avoid any possible carbonation in air (especially for S1-R). A standard potassium chloride solution with an ionic conductivity of 12.888 mS/cm at 25 °C was used to calibrate the electrode before each trial.

The pH of the cement suspensions was monitored using a pH electrode (Mettler Toledo Inlab Expert Pt 1000) connected to a data logger (Consort C3030) at recording time steps of 1 min. As for electrical conductivity measurements, the cement suspensions were continuously mixed using a magnetic stirrer in a sealed vessel. The electrode was calibrated using pH standard buffers at pH 4.1 and 9.2 before each test.

2.2.2. Solution analysis

The concentrations of the aqueous species in the cement suspension containing aluminum nitrate (S1-AlN) were measured using inductively coupled plasma atomic emission spectroscopy (ICP-AES, Thermo Fisher ICAP 6300 Duo) previously calibrated with external standards (solutions of K, Al, B, Mg and P) and matrix reconstitution. Solution aliquots of 1 mL were sampled at relevant hydration times and filtered using a nylon filter with a mesh size of 0.2 μm. They were diluted with HNO_3 (2%) before analysis by ICP-AES. The analytical error was around ±5%.

2.2.3. X-ray diffraction and nuclear magnetic resonance analyses

Hydration of the cement suspension with aluminum nitrate at 20 mmol/L (S1-AlN) was stopped after specific reaction times. The cement suspension was filtered under vacuum using a Büchner funnel. The remaining solids were rinsed with isopropanol, stored at 22 ± 2 °C and 20% relative humidity, and analyzed by X-ray diffraction (XRD) and nuclear magnetic resonance spectroscopy (NMR). The XRD analyses were performed with a Panalytical X'pert Pro device using Cu Kα radiation and

Table 2
Mix designs of the suspensions referring to 1 g of cement ($MgO + KH_2PO_4$).

Sample	Mg/PO_4 molar ratio	w/c ratio	MgO [g]	KH_2PO_4 [g]	Chemicals			Water [g]
					Formula	Amount		
						[mmol/L]	[g]	
S1-R	1	100	0.228	0.772	–	–	–	100
S1-BA	1	100	0.228	0.772	$B(OH)_3$	20	0.124	100
S1-AlN	1	100	0.228	0.772	$Al(NO_3)_3{\cdot}9H_2O$	20	0.75	99.63

the X'Celerator detector. The samples were scanned between 5° and 70° 2θ for 40 min. Further, some samples were characterized using ^{31}P and ^{27}Al MAS-NMR analysis. The ^{31}P NMR spectra were collected on a Bruker Avance I 400 MHz spectrometer (9.4 T) using a probe for 4 mm o.d. zirconia rotors spun at 12.5 kHz. The spectra were recorded at 162 MHz using presaturation followed by a single pulse (π/4, 2.3 μs), recycle delay of 300 or 600 s depending on the sample, 8 transients and proton decoupling at 65 kHz during the acquisition period. The spectra were referenced to H_3PO_4 (85% solution). It should be noted that phosphate crystalline species have an extremely long relaxation delay. Therefore, the relative contribution of crystalline phases in regards to amorphous species was underestimated. The ^{27}Al spectra were recorded at a Larmor frequency of 208.5 MHz using a Bruker Avance III 800 MHz (18.8 T) spectrometer. The samples were spun at 20 kHz in a 3.2 mm probe. The ^{27}Al spectra were made up of 128 free induction decays with a π/10 pulse of 1 μs and a recycle delay of 1 s to ensure quantitative reliability of the intensities observed for the ^{27}Al central transition for sites experiencing different quadrupolar coupling. The chemical shifts were referenced to the external aluminum nitrate solution at 0 ppm.

2.2.4. Thermodynamic modelling

Thermodynamic modelling with the geochemical CHESS software [40] was used to calculate the thermodynamically stable phases in the MKP cement suspensions without/with aluminum nitrate at 20 mmol/L at ambient temperature. The quality of modelling directly depends on the quality and completeness of the underlying database. The Chess database was enriched by adding the recently compiled database of magnesium (potassium) phosphate species [41], as well as (potassium) aluminophosphate species relevant to the investigated system (Table 3).

3. Results

3.1. Electrical conductivity of the suspensions

The evolution of the electrical conductivity of the suspensions is shown in Fig. 1. The reference suspension (S1-R) and that with boric acid (S1-BA) have similar trends with two characteristic peaks (labelled P1 and P2), dividing the cement hydration process into three stages. The first stage (up to P1) is characterized by a rapid increase in the electrical conductivity, indicating domination of MgO dissolution rather than hydrates precipitation [7]. Afterwards, the electrical conductivity decreases slowly in the second stage (between P1 and P2), and more rapidly in the third stage (after P2), when hydrates precipitation becomes the predominant process [7]. Stage II is longer for the suspension with boric acid (S1-BA) than for the reference (S1-R), reflecting a retardation effect on cement hydration. When compared to S1-R, the cement suspension with aluminum nitrate (S1-AlN) shows the missing of stage I, and directly goes through stage II with a sharp decrease in the electrical conductivity. Further, only a small decrease in the electrical conductivity is observed after P2 (stage III). Note that the electrical conductivity is always higher than for suspensions (S1-R) and (S1-BA), which suggests higher concentrations in solution, and can be explained, at least for a part, by the stoichiometry of the salt used ($Al(NO_3)_3$) which releases significant concentrations of nitrates in solution.

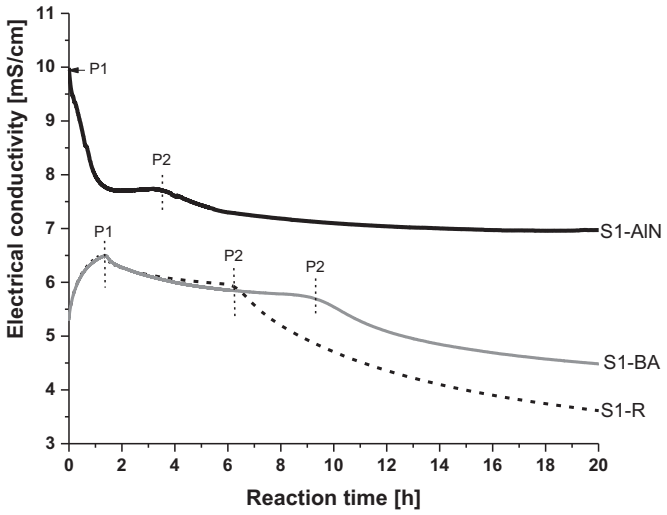

Fig. 1. Typical electrical conductivity curves of the cement suspensions without (S1-R)/with aluminum nitrate (S1-AlN) or boric acid (S1-BA) at 20 mmol/L.

3.2. pH of the suspensions

Fig. 2 shows the pH evolution in the cement suspensions without (S1-R)/with boric acid (S1-BA) or aluminum nitrate (S1-AlN) at 20 mmol/L.

Table 3
(Potassium) aluminophosphate species added to the Chess database.

	Species	Formation reaction	Log K ($T = 25$ °C, $P = 1$ bar)	Ref.
Aqueous	$AlH_2PO_4^{2+}$	$Al^{3+} + H^+ + HPO_4^{2-} \rightarrow AlH_2PO_4^{2+}$	10.31	[42]
	$AlHPO4^+$	$Al^{3+} + HPO_4^{2-} \rightarrow AlHPO_4^+$	7.4	[43]
	$AlPO_4$ (berlinite)	$Al^{3+} + HPO_4^{2-} \rightarrow AlPO_4 + H^+$	7.21	[43]
	$AlPO_4{\cdot}2H_2O$ crystallized (variscite)		9.73	[44]
	$AlPO_4{\cdot}2H_2O$ amorphous (synthetic variscite precipitated from solution)	$Al^{3+} + HPO_4^{2-} + 2\ H_2O \rightarrow AlPO_4\ .2H_2O + H^+$	7.32	[45]
Minerals	$Al_2(PO_4)(OH)_3$ augellite	$2\ Al^{3+} + HPO_4^{2-} + 3\ H_2O \rightarrow Al_2(PO_4)(OH)_3 + 4H^+$	−3.07	[42]
	$Al_3(PO_4)_2(OH)_3{\cdot}5H_2O$ wavellite	$3\ Al^{3+} + 2\ HPO_4^{2-} + 8\ H_2O \rightarrow Al_3(PO_4)_2(OH)_3{\cdot}5H_2O + 5H^+$	2.25	[42]
	$K_3Al_5(HPO_4)_6(PO_4)_2{\cdot}18H_2O$ taranakite	$3\ K^+ + 5\ Al^{3+} + 8\ HPO_4^{2-} + 18\ H_2O \rightarrow K_3Al_5(HPO_4)_6(PO_4)_2{\cdot}18H_2O + 2H^+$	79.94	[44,46]
	$KAl_2(PO_4)_2OH{\cdot}2H_2O$ OH-minyulite	$K^+ + 2\ Al^{3+} + 2\ HPO_4^{2-} + 3H_2O \rightarrow KAl_2(PO_4)_2OH{\cdot}2H_2O + 3\ H^+$	16.32	[44]

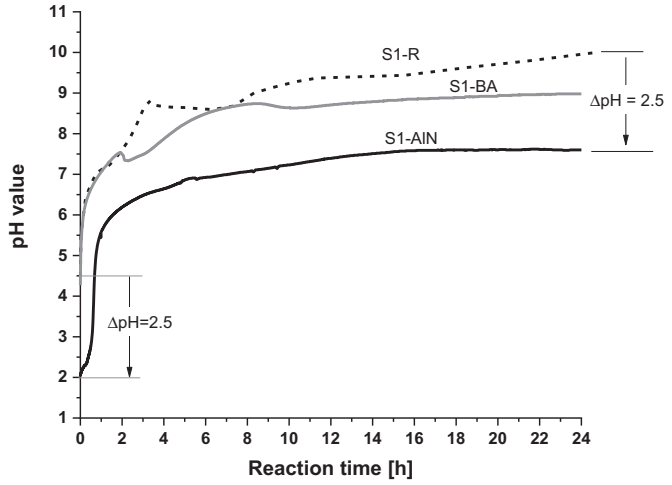

Fig. 2. Evolution of pH in the cement suspensions without (S1-R)/with aluminum nitrate (S1-AlN) or boric acid (S1-BA) at 20 mmol/L. Data are taken from [7] for S1-R.

Data are taken from [7] for reference cement suspension S1-R. The addition of boric acid or aluminum nitrate to the suspension leads to a pH decrease. Moreover, aluminum nitrate shows a stronger pH reduction effect, which causes initial and final pH drops of ≈2.5 units as compared to the reference suspension (S1-R).

3.3. Aqueous concentrations

The concentrations of the aqueous species in the cement suspensions without (S1-R)/with boric acid (S1-BA) or aluminum nitrate (S1-AlN) are shown in Fig. 3 and Table 4. To compare the retardation mechanisms by boric acid and aluminum nitrate, the cement suspension with boric acid (S1-BA) is used as a reference in addition to cement suspension S1-R. Data for S1-R and S1-BA are both taken from [7]. The magnesium concentrations in S1-R and S1-BA show similar trends: they first increase rapidly to their maximum within the first hour and then quickly drop to several mmol/L (Fig. 3 A). In the cement suspension with aluminum nitrate (S1-AlN), magnesium is initially released at the same rate (Table 4); however, unlike S1-R and S1-BA, it continues to accumulate in solution, reaches a peak concentration close to 37 mmol/L after 3 h, and finally decreases. The potassium concentration in S1-R1 and S1-BA shows a decrease in two steps, separated by a transient increase between 5 h and 8.33 h (S1-R) or between 6 h and 10 h (S1-BA) (Fig. 3B, Table 4). This non monotonous evolution has been explained by a multi-stage process involving precipitation (reaction 2) and dissolution of $Mg_2KH(PO_4)_2{\cdot}15H_2O$ (reaction 3), as well as precipitation of K-struvite (reaction 4) [7].

$$2\,Mg^{2+} + 2\,H_2PO_4^- + K^+ + 15\,H_2O \rightarrow Mg_2KH(PO_4)_2{\cdot}15H_2O + 3H^+ \qquad 7.2 \le pH \le 8.6 \tag{2}$$

$$Mg_2KH(PO_4)_2{\cdot}15H_2O + H^+ \rightarrow 2Mg^{2+} + K^+ + 2HPO_4^{2-} + 15H_2O \quad pH > 8.6 \tag{3}$$

$$MgO + K^+ + HPO_4^{2-} + 6H_2O \rightarrow MgKPO_4{\cdot}6H_2O + OH^- \qquad pH > 8.6 \tag{4}$$

The first decrease in the K concentration is attributed to the precipitation of $Mg_2KH(PO_4)_2{\cdot}15H_2O$ (reaction 2), the transient increase to the predominant dissolution of $Mg_2KH(PO_4)_2{\cdot}15H_2O$ (reaction 3) over precipitation of K-struvite, and the final decrease to the precipitation of K-struvite which becomes the main process. With aluminum nitrate, the K concentration exhibits a different evolution, with a decrease in the first 3 h and very little change afterwards.

In contrast to potassium, phosphorus is consumed faster in S1-AlN than in S1-R and S1-BA (Fig. 3C), and its concentration falls below the detection limit after 24 h. Note however that, as for S1-R and S1-BA, the P concentration decreases in two steps, with a plateau observed between 1 h and 3 h. The Al concentration sharply decreases in the early stages of hydration and is below the detection limit after 1 h only. Its behavior is thus very different from that of boron which remains fully dissolved in solution (Fig. 3D).

3.4. XRD analyses

The solid assemblages formed in the reference cement suspension (S1-R) after different reaction times were documented in detail in [7]. Fig. 4 shows the diffraction patterns of the solid fraction of suspension S1-AlN after several selected reaction times. During the first hour, no crystalline hydrates are observed, but some amorphous phases may be present, as evidenced by humps centered at 2θ CuKα 17° and 29° for the 10 min-old and 1 h-old samples. Newberyite is detected from 4.8 h, along with a clear consumption of magnesia. After 24 h, a mix of cattiite (major phase), newberyite (minor phase), and some unidentified amorphous phase is pointed out, while magnesia is almost fully depleted.

3.5. NMR analyses

The ^{31}P and ^{27}Al MAS-NMR spectra of the solid fraction of suspension S1-AlN are shown in Fig. 5 after increasing hydration times. After 24 h, the ^{31}P NMR spectrum of the reference cement suspension (S1-R) shows two peaks close to 7 and 6.5 ppm (Fig. 5A), which are assigned to cattiite and K-struvite [8,25], respectively. These two phases were also evidenced by XRD in [7]. At the early reaction time of 1 h, the cement suspension with aluminum nitrate at 20 mmol/L (S1-AlN) shows a broad hump over the range of around 3 to −26 ppm and centered around −12 ppm, indicating amorphous orthophosphates bonded to aluminum [47,48]. The on-going reaction leads to significant changes on the ^{31}P spectrum after 24 h, where two strong peaks are displayed at ~7.0 and ~−7.4 ppm, suggesting the formation of cattiite and newberyite [8], respectively. However, when compared with S1-R, the characteristic resonance for K-struvite is missing, which is in good agreement with the XRD results in Fig. 4. Moreover, after 24 h, the amorphous hump is still observed over the same range of chemical shifts as for the 1 h sample, but with a lower intensity. The ^{27}Al spectra of S1-AlN after different reaction times are displayed in Fig. 5B. The main information derived from the chemical shift of aluminum concerns the coordination number. It is possible to discriminate between tetrahedral environments (shifts between 50 and 100 ppm), pentahedral environments (25 to 40 ppm), and octahedral environments (−10 to 20 ppm) [49]. A main peak is evidenced at ~−7 ppm, a minor one at ~48 ppm, and a trivial hump centered at ~23 ppm. They correspond to aluminum atoms in 6- (Al[VI]), 4- (Al[IV]), and 5- (Al[V]) fold coordination by oxygen respectively [48,50–52]. Analysis of the ^{27}Al MAS NMR spectra is complicated by quadrupolar broadening which can yield asymmetric peaks. For spectral decomposition, two Gaussian/Lorentzian lines were used to fit the peaks assigned to aluminum in octahedral and tetrahedral

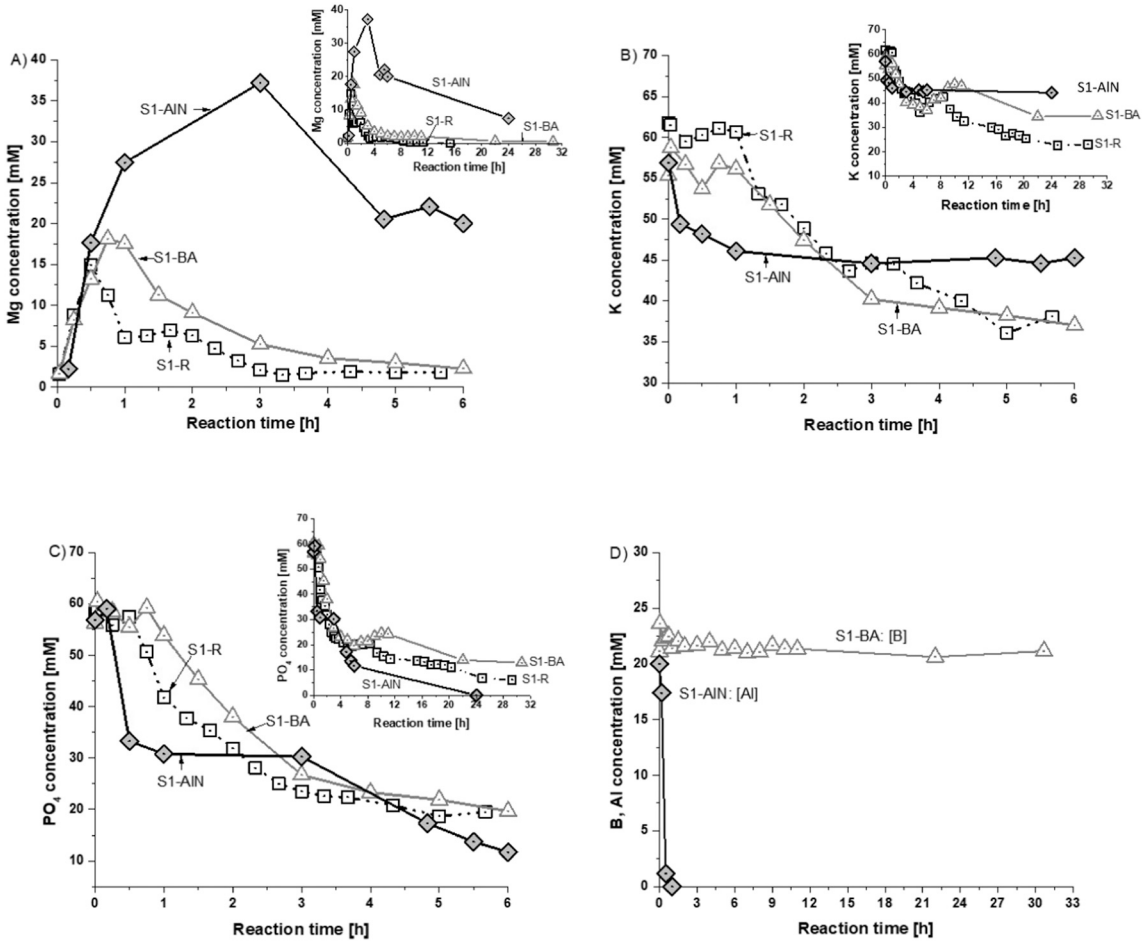

Fig. 3. Aqueous concentrations (mmol/L) in the cement suspensions without (S1-R)/with boric acid (S1-BA) or aluminum nitrate (S1-AlN). Data of S1-R and S1-BA were taken from [7].

Table 4
Summary of the measured aqueous concentrations in the cement suspensions without (S1-R)/with boric acid (S1-BA) or aluminum nitrate (S1-AlN) after selected reaction times.

Time [h]	S1-R [7], [mmol/L]				Time [h]	S1-BA [7], [mmol/L]					Time [h]	S1-AlN, [mmol/L]				
	Mg	K	P	pH		Mg	K	P	B	pH		Mg	K	P	Al	pH
0	n.d.	61.8	58	4.5	0	n.d.	55	56	21	4.2	0	n.d.	57	57	20	2.0
0.25	8.85	60	56	6.4	0.25	8.2	57	59	22	6.3	0.17	2	49	59	17	2.3
0.75	11	61	51	7.0	0.75	18	57	59	22	6.9	0.5	18	48	33	1.2	2.8
1.33	6.3	53	38	7.20	1	18	56	54	21	7.1	1	27	46	31	n.d.	5.6
3	2.	45	24	8.6	1.5	11	52	45	22	7.4	3	37	45	30	n.d.	6.5
5	1.8	36	19	8.6	3	5.2	40	27	22	7.5	4.83	21	45	17	n.d.	6.8
8.33	0.63	43	20	9.0	4	3.5	39	23	22	7.9	5.5	22	45	14	n.d.	6.9
9.33	0.43	37	17	9.2	5	3.0	38	22	21	8.2	6	20	45	12	n.d.	6.9
11.33	0.31	32	15	9.4	6	2.3	37	20	21	8.5	24	7.5	44	n.d.	n.d.	7.6
15.33	n.d.	30	14	9.4	8	2.0	42	21	21	8.7						
20.33	n.d.	25	11	9.7	10	2.1	48	25	21	8.6						
24.87	n.d.	23	6.9	10.0	22	0.64	34	14	21	9.0						

Note: Data of S1-R and S-BA were taken from [7]. n.d.: under detection limit, not detected.

coordination (Fig. 6). The chemical shifts and full widths at half maximum were kept as constant as possible from one spectrum to another (Appendix B). Fig. 7 shows that the populations of aluminum in tetrahedral, pentahedral and octahedral coordinations do not evolve notably during the hydration process. The peaks assigned to octahedral aluminum, and possibly to tetrahedral aluminum, seem however to slightly shift upfield with ongoing hydration (Fig. 5B).

4. Discussion

4.1. Type of aluminophosphate precipitating during cement hydration

4.1.1. Evolution of aqueous concentrations

The evolution of the aqueous concentrations and the decrease in the ionic conductivity suggest the rapid formation of an aluminophosphate

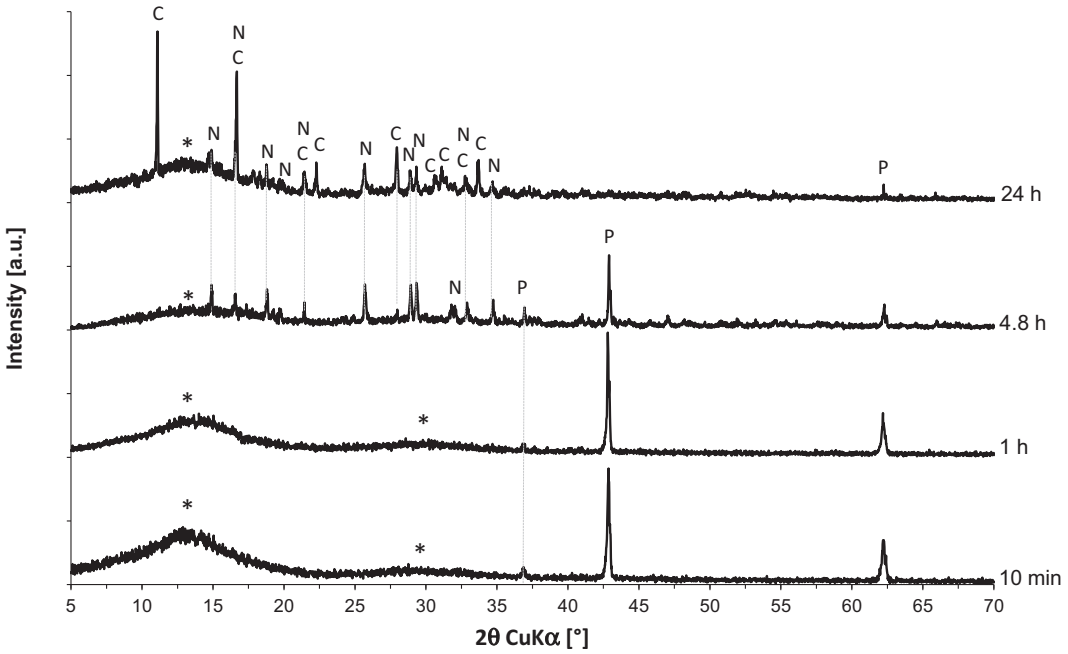

Fig. 4. XRD patterns of the cement suspension with aluminum nitrate at 20 mmol/L (S1-AlN) after different reaction times. C = cattiite ($Mg_3(PO_4)_2{\cdot}22H_2O$); N = newberyite ($MgHPO_4{\cdot}3H_2O$); P = periclase (MgO); * = amorphous phase(s).

phase within the first hour. The amorphous nature of the precipitate is evidenced by ^{31}P MAS-NMR and XRD results, with broad humps typical of poor crystalline order. If we assume that precipitation of this mineral is responsible from the decrease in the P, K and Al concentrations in solution, some mass balance calculations show that the solid formed would have P/Al and K/Al molar ratios within the ranges [1.25; 1.33] and [0.46; 0.6] respectively (Fig. 8).

These ratios can be compared to those of well-known potassium alumino-phosphate minerals. Most of them have been described in studies aiming at understanding reactions between soil clays and phosphate-containing fertilizers or phosphate-rich excrements of birds, penguins or bats [53,54]. The reaction of clay minerals with potassium and phosphate solutions under various conditions of pH and temperature produces a couple of crystalline products:

- Taranakite ($K_3Al_5(HPO_4)_6(PO_4)_2{\cdot}18H_2O$) [55,56], which can partly dehydrate to Francoanellite $K_3Al_5(HPO_4)_6(PO_4)_2{\cdot}12H_2O$ [57];
- OH-Minyulite $KAl_2(PO_4)_2(OH){\cdot}4H_2O$ (an analogous to Minyulite mineral $KAl_2(PO_4)_2(OH,F){\cdot}4H_2O$ where fluoride ions are fully replaced by hydroxide ions) [58–60], or its less hydrated form $KAl_2(PO_4)_2(OH){\cdot}2H_2O$ (with two polymorphs belonging to orthorhombic or monoclinic crystal systems) referred as Tinsleyite but also as OH-Minyulite [56,60–62];
- $KAl(HPO_4)_2{\cdot}H_2O$ [63].

Taranakite readily forms when clay minerals react with sodium and phosphate-containing solutions [56], but it can also be synthesized by reaction of $AlCl_3$ with H_3PO_4 and KOH [55]. Haseman et al. [58] observed taranakite in phosphate solutions with a pH comprised between 1.7 and 5.5. However, Gossner reported that taranakite, rapidly formed from gibbsite at pH 2, later transforms into $KAl(HPO_4)_2{\cdot}H_2O$ [56]. In their investigation of the degradation of kaolinite in a phosphate-rich environment, Dick et al. [63] also noticed the formation of $KAl(HPO_4)_2{\cdot}H_2O$ at pH $\leq$ 2. In the pH range 2.2–2.6, mixtures of taranakite and $KAl(HPO_4)_2{\cdot}H_2O$ were observed, whereas taranakite was the sole product at pH $>$ 2.6. The authors noted however a difference between the experiments with clay minerals and the syntheses by precipitation from aluminum salt, phosphoric acid and potassium phosphate. In the latter case, an amorphous potassium aluminophosphate precipitated readily, and then slowly crystallized. At pH 2, crystallization of $KAl(HPO_4)_2{\cdot}H_2O$ was first noticed, but with prolonged treatment, this phase finally transformed into taranakite contrarily to clay experiments. Dick et al. [56] later confirmed that taranakite seems to be the stable product at pH 4 and temperatures comprised between 293 and 373 K. It also forms at pH 5.5 as a metastable product which transforms with time into OH-minyulite $KAl_2(PO_4)_2(OH){\cdot}nH_2O$ (n = 2 or 4 depending on the temperature).

In our work, the pH increases from 2.1 to 6.5 during the first 3 h (Fig. 2), thus evolving from conditions favorable to the precipitation of taranakite or $KAl(HPO_4)_2{\cdot}H_2O$ to conditions favorable to the formation of OH-minyulite. The K/Al and P/Al ratios of the solid formed experimentally are notably lower than 1 and 2 respectively, making the precipitation of $KAl(HPO_4)_2{\cdot}H_2O$ unlikely (Fig. 8). However, these ratio values are intermediate between or close to those of taranakite and OH-minyulite, and do not allow to discriminate between these two phases.

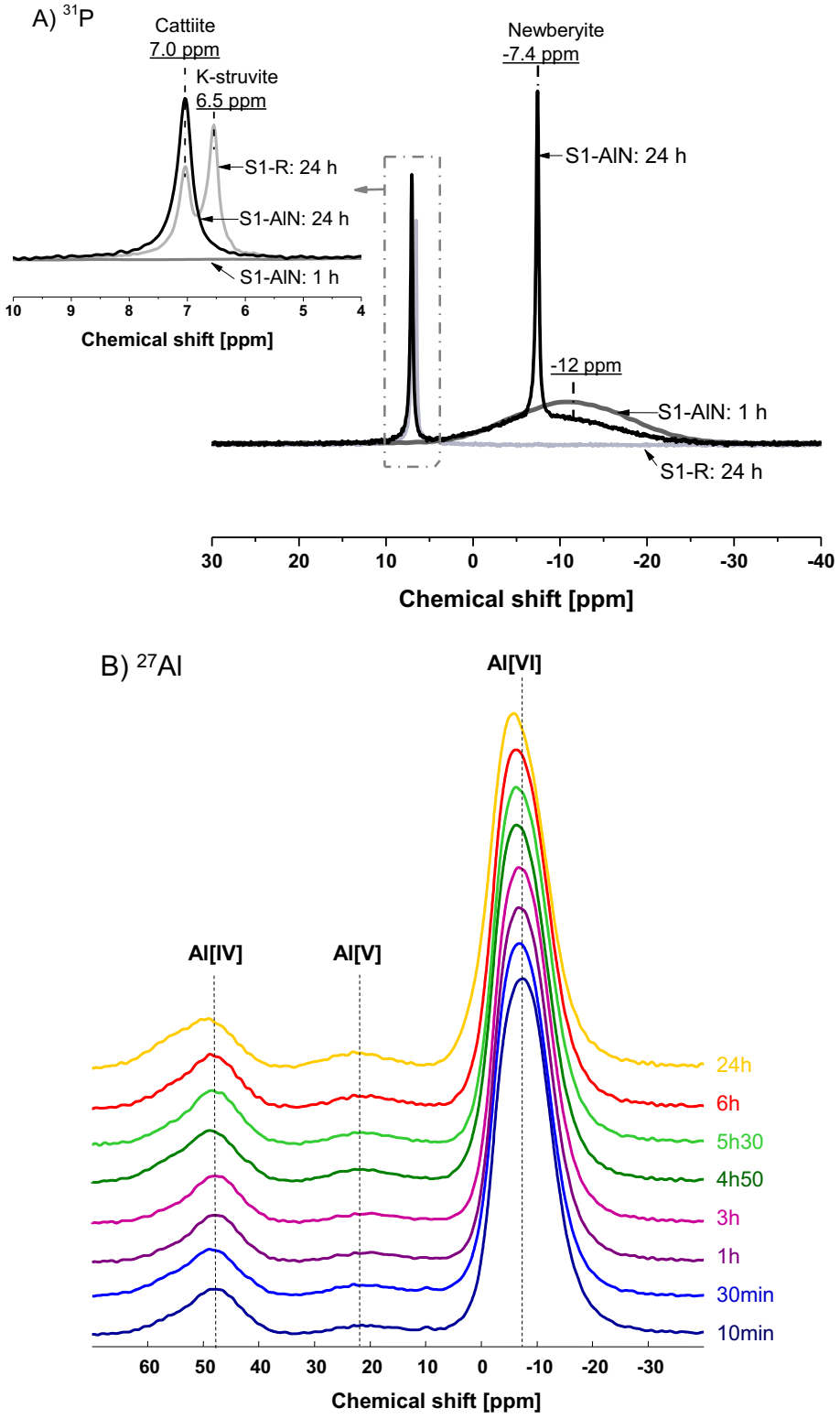

Fig. 5. Proton-decoupled ^{31}P (A) and ^{27}Al (B) MAS-NMR spectra of the solid fractions of suspensions S1-R and S1-AlN after different reaction times.

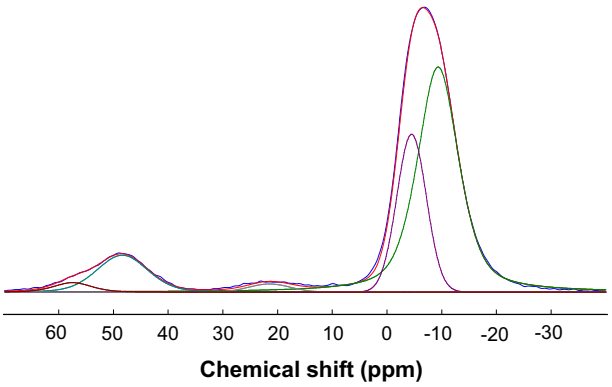

Fig. 6. Example of decomposition of ^{27}Al NMR spectra – solid fraction of the 10 min-old suspension.

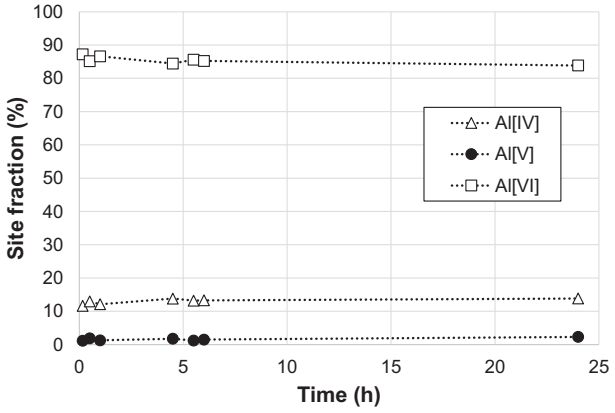

Fig. 7. Populations of the IV-, V- and VI-coordinated aluminum atoms in the solid fraction of suspension S1-AlN obtained from profile fitting of the ^{27}Al MAS-NMR spectra recorded from 10 min to 24 h.

4.1.2. NMR experiments

NMR results can be reexamined to gain more information about the type of aluminophosphate formed in our experiments. Table 5 summarizes the chemical shifts reported in the literature for various aluminophosphate minerals characterized by ^{27}Al and/or ^{31}P MAS-NMR. In this work, the broadness of the peaks, resulting from the amorphous character of the samples up to 4 h, makes their assignment difficult, especially for the ^{31}P spectra. The peak for orthophosphate lies from $\delta = 5$ ppm to $\delta = -25$ ppm. This interval includes the chemical shifts of all the hydrated aluminophosphate phases from Table 5. The peak observed for octahedral aluminum ranges from $\delta \approx 3$ ppm to $\delta \approx -20$ ppm, which could be consistent with the presence of several hydrates: variscite $AlPO_4{\cdot}2H_2O$ ($\delta = -9$ ppm), taranakite $K_3Al_5(HPO_4)_6(PO_4)_2{\cdot}18H_2O$ ($\delta = -8.9$ ppm), but also $Al(H_2PO_4)(HPO_4){\cdot}3H_2O$ ($\delta = -7.6$ ppm), and possibly $Al(H_2PO_4)_3$ ($\delta = -16.6$ ppm), no data being available for OH-minyulite. Nevertheless, the spectra make it possible to reject the hypothesis of precipitation of aluminum hydroxide with adsorbed phosphate ions. Klein et al. [64] have shown indeed that this product has a chemical shift at $\delta \approx 8$ ppm (as gibbsite or boehmite), but no peak is observed at such chemical shift in the present study.

It must be outlined that tetrahedral Al, evidenced in this work, is not observed on the ^{27}Al MAS-NMR spectra of variscite, taranakite or F-minyulite. Similarly, refinement of the crystal structure using Rietveld analysis has shown that OH-minyulite only contains one type of Al sites with octahedral coordination [59,60]. The question of the Al[IV] peak origin in our experiments is thus raised. Interestingly, two papers report ^{31}P and ^{27}Al spectra very similar to those obtained in this work.

- Lookman et al. [48] synthesized an aluminum phosphate gel by adding dropwise a 0.5 M NaOH solution to a solution containing $AlCl_3{\cdot}6H_2O$ (5 g/L) and KH_2PO_4 (9 g/L) until pH 3.8. The suspension was allowed to stand overnight, before being washed with deionized water, centrifuged and dried at 70 °C. The resulting product was X-ray amorphous. Its ^{31}P spectrum exhibited one broad peak, indicating the existence of different unresolved chemical environments, with a maximum intensity at ~−12 ppm, as observed in this work (Fig. 5). Its ^{27}Al spectrum showed one main peak at ~−10 ppm, assigned to octahedral aluminum coordinated with one or more P atoms, and asymmetric due to a second order quadrupolar effect. The

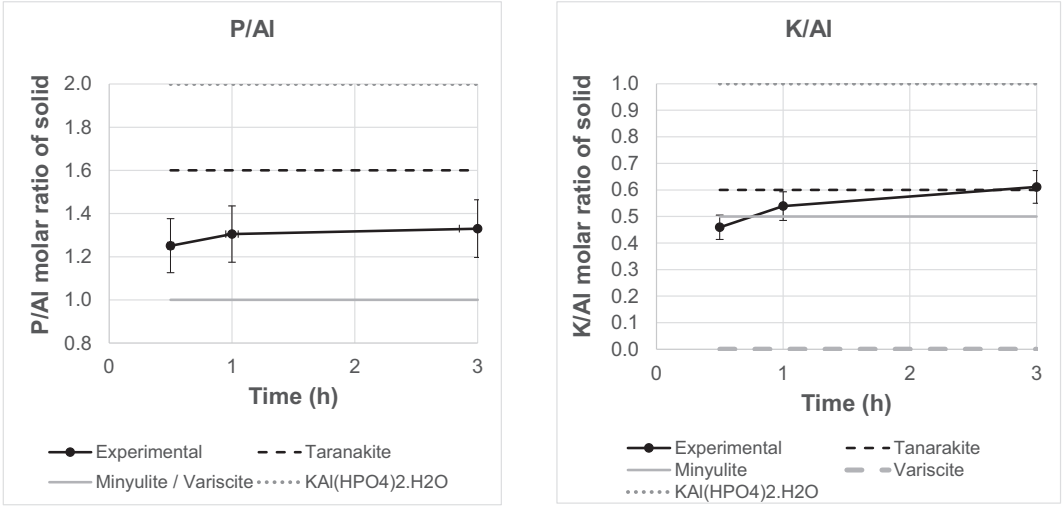

Fig. 8. Comparison of the P/Al and K/Al molar ratios of the solid formed during the first 3 h of hydration with those of well-known aluminophosphate minerals (Variscite $AlPO_4{\cdot}2H_2O$, Taranakite $K_3Al_5H_6(PO_4)_8{\cdot}18H_2O$, OH-Minyulite $KAl_2(PO_4)_2(OH){\cdot}4H_2O$, and $KAl(HPO_4)_2{\cdot}H_2O$).

Table 5
^{27}Al and ^{31}P MAS NMR results from the literature for aluminophosphate minerals.

Mineral		^{27}Al			^{31}P	
Formula	Name	Chemical shift (ppm)	Al atom coordination	Ref.	Chemical shift (ppm)	Ref.
AlOOH	Boehmite	8.0 (7.05 T)	Octahedral	[64]		
$Al(OH)_3$ amorphous		6.0 (9.4 T)	Octahedral	[48]		
$Al(OH)_3$	Gibbsite	8.1 (9.4 T)	Octahedral	[67]		
		8.0 (9.4 T)		[68]		
$AlPO_4$	Berlinite	40 (7.05 T)	Tetrahedral	[64]	−28	[70]
		39.5 (6.4 T)		[69]	−24.8	[71]
		39.7 (6.4 T)		[69]	−25.3	[72]
		36		[70]		
		33.2 (4.7 T)		[71]		
$Al(PO_4)\cdot 2H_2O$	Variscite	−9 (7.05 T)	Octahedral	[64]	−18.6	[73]
					−19.2	[72]
$Al(PO_4)\cdot 2H_2O$	Metavariscite	−13.2 (4.7 T)	Octahedral	[71]	−19.3	[71]
$Al(H_2PO_4)_3$		−16.6 (6.4 T)	Octahedral	[69]		
$Al(H_2PO_4)(HPO_4)\cdot 3H_2O$		−7.6 (6.4 T)	Octahedral	[69]		
$Al_3(OH)_3(PO_4)_2\cdot 5H_2O$	Wavellite				−11.2	[72]
$Al_2(OH)_3(PO_4)\cdot H_2O$	Senegalite				−16.2	[72]
$Al_2(OH)_3(PO_4)$	Augelite				−29.6	[72]
$K_3Al_5(HPO_4)_6(PO_4)_2\cdot 18H_2O$	Taranakite	−8.9 (11.75 T)	Octahedral	[74]	4.5; −18	[74]
					5.2; −17.3	[56]
$KAl(HPO_4)_2\cdot H_2O$					−6.5; −10.7; −12.6	[63]
$KAl_2(PO_4)_2(OH)\cdot 4H_2O$	OH-Minyulite				−9.6	[60]
$KAl_2(PO_4)_2(OH)\cdot 2H_2O$					−6.9; −18.7	[63]
$KAl_2(PO_4)_2F\cdot 4H_2O$	F-Minyulite	−2.1	Octahedral		−11.2	[75]

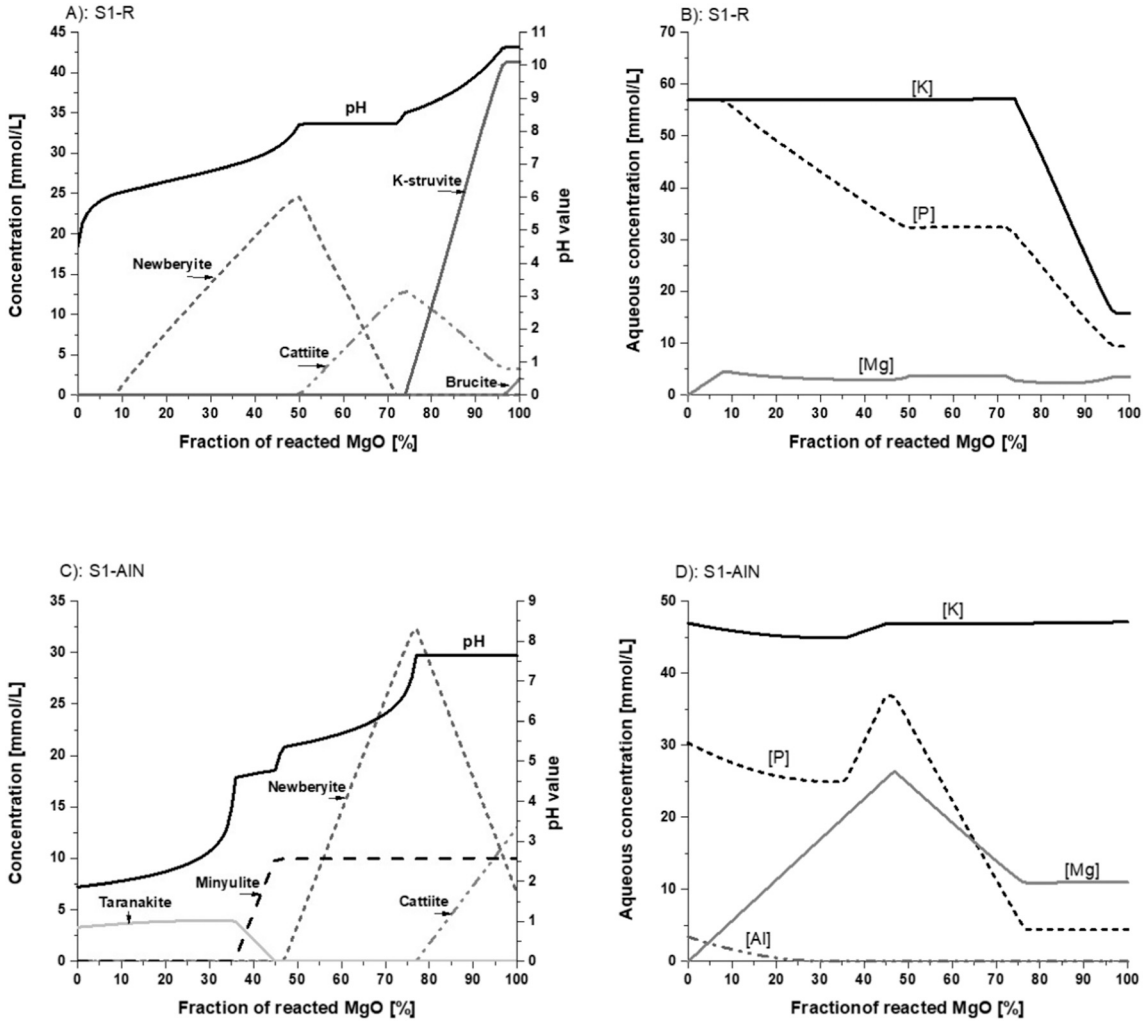

Fig. 9. Thermodynamic modelling of the hydration process in suspensions S1-R (A: solid phases and pH, B: aqueous concentrations) and S1-AlN (C: solid phases and pH, B: aqueous concentrations).

second peak, at a chemical shift of about 40 ppm, was typical of Al tetrahedrally bound to 4 P atoms via oxygen atoms.

- Similarly, Klein et al. [64] synthesized some aluminum hydroxyphosphate vaccine adjuvants by adding sodium hydroxide to a solution containing potassium aluminum phosphate, sodium chloride and sodium phosphate to get pH values comprised between 2.5 and 6.8. The syntheses performed with a target P/Al ratio of 1.3 yielded an amorphous product with an effective P/Al ratio close to 1.1. Unfortunately, its alkali content was not determined. Its ^{27}Al NMR spectrum contained two peaks at chemical shifts corresponding to tetrahedral and octahedral aluminum. As in this work, the peak of Al [VI] was predominant, with a peak intensity about 4 times higher than that of Al[IV], and its chemical shift varied slightly as a function of the precipitation pH from ~−9.5 ppm at pH 3 to ~−7 ppm at pH 7. Such variation has been attributed to modest compositional changes resulting from the increased ability of hydroxyl ions to compete with phosphate for aluminum binding at higher pH [44–46]. As for the small peak assigned to tetrahedral aluminum, no correlation could be established between its intensity and the precipitation pH or the phosphate content.

Three main hypotheses can be considered to assign the Al[IV] peak.

(i) In a subsequent paper, Lookman et al. [65] postulated that the precipitated product was $Al(OH)_2HPO_4$, but without giving any experimental evidence of such composition. In this work, precipitation of $Al(OH)_2HPO_4$ seems unlikely since it cannot account for the amounts of K, Al and P depleted from solution over the first 3 h of reaction.

(ii) Lookman et al. [65] have also postulated that octahedral aluminum can partly, and reversibly to some extent, transform into tetrahedral aluminum upon drying. Nevertheless, Klein et al. [64] characterized dry and wet amorphous aluminophosphate products (showing the same spectra as in this study), and observed in both cases some Al in tetrahedral environment, which contradicts this second hypothesis of Al[IV] formation upon drying.

(iii) More likely, the small fraction of Al[IV] would result from the very rapid precipitation of the amorphous phase, producing a disordered structure. This has already been observed for gibbsite [66]: well-crystallized gibbsite only contains octahedral environment, whereas rapidly precipitated amorphous aluminum hydroxide not only comprises AlO_6 subunits, but also AlO_4 and even AlO_5 units bound through hydrogen bonds with a wide distribution of bonding strengths.

To conclude, the exact nature of the potassium aluminophosphate formed at early age cannot be determined from the NMR results because of the broadness of the peaks resulting from the amorphous character of this product. The spectra are not uncompatible with the precipitation of an amorphous precursor of taranakite or minyulite, but lead to reject the hypothesis of the precipitation of amorphous aluminum hydroxide sorbing phosphate and potassium ions.

4.1.3. Thermodynamic modelling

The sequence of precipitations occurring in cement suspensions without (S1-R) or with aluminum nitrate at 20 mmol/L (S1-AlN) was investigated using thermodynamic modelling. Fig. 9A shows that newberyite ($MgHPO_4{\cdot}3H_2O$) is the first phase to precipitate from the reference cement suspension (S1-R) through reaction (5).

$$MgO + H_2PO_4^- + 3H_2O \rightarrow MgHPO_4{\cdot}3H_2O + OH^- \quad (5)$$

The pH increase in the cement suspension leads to the transformation of newberyite into cattiite ($Mg_3(PO_4)_2{\cdot}22H_2O$) according to reaction (6).

$$3\ MgHPO_4{\cdot}3H_2O + 3OH^- + 10\ H_2O \rightarrow Mg_3(PO_4)_2{\cdot}22H_2O + PO_4^{3-} \quad (6)$$

At pH above 8.5, K-struvite precipitates following reaction (4).

Moreover, with sufficient potassium and phosphate ions in the cement suspension, cattiite is predicted to partially destabilize to K-struvite through reaction (7).

$$Mg_3(PO_4)_2{\cdot}22H_2O + 3\ K^+ + PO_4^{3-} \rightarrow 3MgKPO_4{\cdot}6H_2O + 4H_2O \quad (7)$$

In addition, traces of brucite are predicted to form when the pH reaches 10.5.

This sequence of precipitation agrees well with the experimental results [7], except for the prediction of newberyite instead of $Mg_2KH(PO_4)_2{\cdot}15H_2O$ as the transient phase. The final pH is fairly well reproduced (calculated pH of 10.5, measured pH of 10.1), as well as the final K concentration (calculated concentration of 15.8 mmol/L, measured concentration of 16.3 mmol/L) (Fig. 9B). The P and K concentrations are however a bit overestimated by the calculation.

With aluminum nitrate (S1-AlN), thermodynamic modelling in Fig. 9C shows a decrease in the initial and final pH values as compared to the reference cement suspension (S1-R), which is in good agreement with the experimental results (Fig. 3). Taranakite precipitates according to reaction (8) at the very beginning of the hydration process, and is then destabilized at the expense of OH-minyulite when the pH reaches 4.6 (reaction 9).

$$3\ K^+ + 5\ Al^{3+} + 8\ H_2PO_4^- + 18\ H_2O \rightarrow K_3Al_5(HPO_4)_6(PO_4)_2{\cdot}18H_2O + 10H^+ \quad (8)$$

$$2\ K_3Al_5(HPO_4)_6(PO_4)_2{\cdot}18H_2O \rightarrow 5\ KAl_2(PO_4)_2(OH){\cdot}4H_2O + K^+ + 6\ HPO_4^{2-} + 11H_2O + 11\ H^+ \quad (9)$$

This precipitation sequence is consistent with the experimental observations of Dick et al. [56] showing that the stable phase is taranakite at pH 4, and OH-minyulite at pH 5.5. It must be mentioned that the solubility product of amorphous variscite reported by Veith and Sposito [45] has been used for the calculation since, according to these authors,

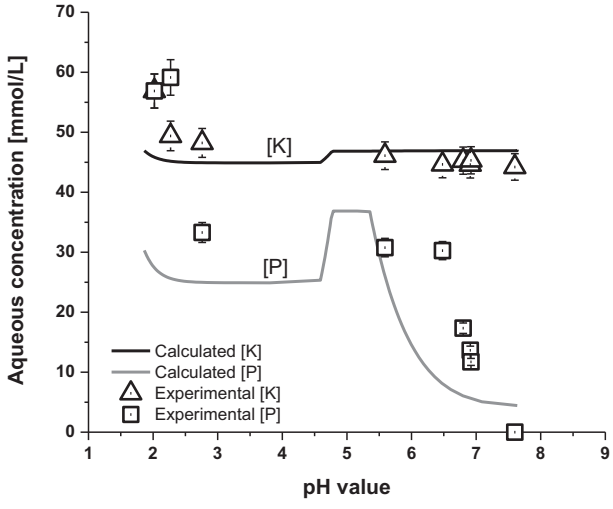

Fig. 10. Comparison between calculated and predicted aqueous P and K concentrations as a function of pH.

there is no conclusive evidence of the precipitation of well-crystallized variscite at ambient temperature in soils in contact with fertilizers. The same calculation using the solubility product of crystallized variscite leads to its initial precipitation from pH 1.9 to 2, but this phase in then destabilized at the expense of taranakite.

For MgO reaction degrees of less than 45%, only aluminophosphate phases are predicted to precipitate and the magnesium ions released by the dissolution of MgO accumulate in solution. This would support the hypothesis of Section 4.1.1 considering that the consumption of Al, K and P ions from solution at early age reflects the stoichiometry of the precipitated aluminophosphate phase. Precipitation of cattiite at the expense of newberyite occurs when the pH reaches 7.6. The modelling reproduces fairly well some experimental observations: the initial and final pH values (2.0 and 7.6 respectively), the initial precipitation of a potassium aluminophosphate, the later precipitation of newberyite and cattiite, as well as the final Al and K concentrations (Fig. 9.D). The final P and Mg concentrations are however a bit overestimated, as for the reference suspension. The transformation of taranakite into OH^--minyulite in suspension S1-Al, as predicted by the model, cannot be ascertained. Gossner reported indeed that metastable taranakite precipitated at pH 5.5 evolves slowly to OH-minyulite [56]. Besides, the crystallinity of the precipitated aluminophosphates is too poor to enable their accurate assignment. To get rid of the time variable, the aqueous P and K concentrations measured experimentally and calculated by the model were plotted as a function of pH (Fig. 10). The transformation of taranakite into OH-minyulite should produce an increase in the K concentration, but of the same magnitude as the analytical error, and a transient and more important increase in the P concentration. This latter was not evidenced experimentally, but these results should be confirmed by increasing the number of sampling points between 3 and 6 h.

4.2. Retardation of cement hydration by aluminum nitrate

Thanks to the better understanding the processes occurring during hydration of MKP cement in the presence of aluminum nitrate, it is possible to put forward several hypotheses to explain the retardation effect of this salt. When compared with S1-R, a higher reaction degree of MgO has to be reached in S1-AlN to get the precipitation of newberyite, and later its partial transformation into cattiite (Fig. 9). This is due to the following reasons:

- The acidic nature of aluminum nitrate which reduces the initial pH by two units (Fig. 2).
- The lower phosphate concentration in solution due to the initial precipitation of a taranakite-like amorphous product, meaning that higher Mg concentrations are needed to reach the solubility limit of newberyite.
- A salt effect: since Al^{3+} cations and a fraction of K^+ cations are depleted from solution by the precipitation of the taranakite-like amorphous product, other cations must balance the negative charges of nitrate ions which remain dissolved in solution. Electric balance is obtained by an increase in the dissolved H^+ and Mg^{2+} concentrations, as well as in the K^+ concentration in the later stage of hydration (Figs. 2 and 3).

The salt effect is also the main process postulated to explain the retardation by boric acid in suspension [7]. As the pH increases, boric acid, which remains fully dissolved in solution, is partly ionized into borate ions and electrical balance is maintained by an increase in the cations concentrations (Mg^{2+}, K^+ and H^+). The higher potassium solubility tends to promote the precipitation of cattiite, a potassium-free hydrate, at the expense of K-struvite. With aluminum nitrate, the precipitation of K-struvite is even prohibited under the conditions of this work, which can be attributed to a higher salt effect (the nitrate concentration is constant at 60 mmol/L whereas the $B(OH)_4^-$ concentration reaches 8 mmol/L at pH 9) and to the competitive precipitation of the amorphous potassium aluminophosphate.

5. Conclusion

In this study, aluminum nitrate was considered as a potential alternative to boron compounds as a set retarder for MKP cement. The influence of aluminum nitrate on hydration of a MKP cement suspension at a Mg/PO_4 molar ratio of 1 and a w/c ratio of 100 was investigated using both experimental and thermodynamic modelling approaches. When compared with the reference cement suspension with the same Mg/PO_4 and w/c ratios, the use of aluminum nitrate leads to an instant drop of the electrical conductivity in the cement suspension, and decreases the suspension pH. These observations result from the precipitation of an amorphous potassium aluminophosphate which may be a precursor of taranakite ($K_3Al_5(HPO_4)_6(PO_4)_2{\cdot}18H_2O$). Moreover, under the investigated conditions, aluminum nitrate prohibits the precipitation of potassium-containing magnesium phosphate hydrates, e.g. $Mg_2KH(PO_4)_2{\cdot}15H_2O$ and K-struvite, and delays the formation of newberyite and the later-on transformation to cattiite (Fig. 11). In addition, the thermodynamic modelled phase development with the ongoing cement hydration agrees rather well with the experimental findings. Future work will be focused on the influence of aluminum nitrate on MKP cement hydration at lower w/c ratio, with a twofold objective: *(i)* determine whether the precipitation of K-struvite is also precluded under these conditions, and *(ii)* assess the influence of the admixture on the properties of the hardened cement paste (mechanical properties, volume stability).

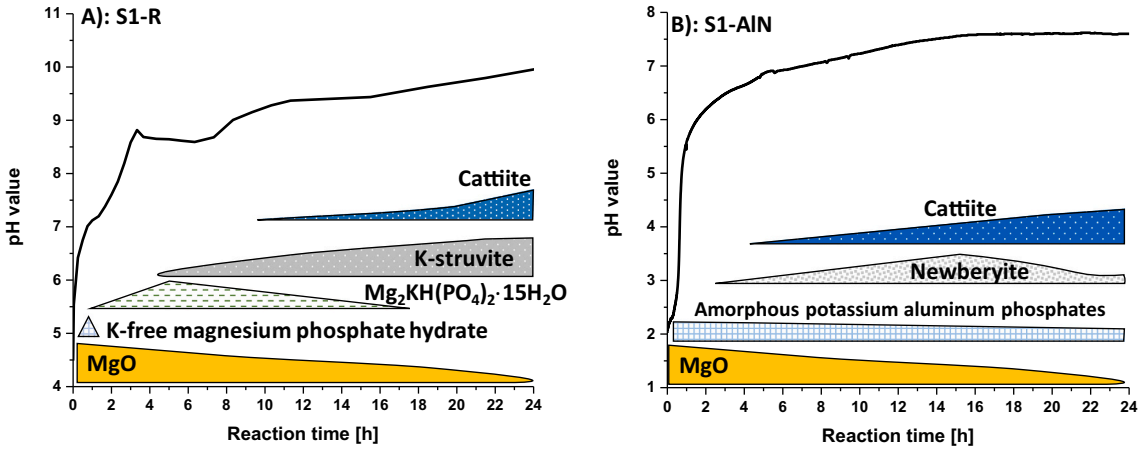

Fig. 11. Schematic hydration paths of the cement suspensions without (S1-R)/with aluminum nitrate (S1-AlN).

CRediT authorship contribution statement

Céline Cau Dit Coumes: conceptualization, methodology, resources, data curation, writing (original draft), review and editing, supervision, funding acquisition.

Angélique Rousselet: investigation, validation, data curation.

Biwan Xu: investigation, data curation, writing (original draft).

Cyrille Albert-Mercier: investigation, data curation (NMR experiments).

Sandrine Gauffinet: conceptualization, supervision, funding acquisition, project administration.

Declaration of competing interest

The authors declare that they have no known competing financial interests or personal relationships that could have appeared to influence the work reported in this paper.

Appendix A. Final setting results of fly ash blended pastes without (P1-FA-R) or with aluminum nitrate (P1-FA-AlN)

Sample	Mg/PO_4 molar ratio	w/c ratio	Cement		FA [g]	$Al(NO_3)_3·9H_2O$		Water [g]	t_{FS}[b] [h]
			MgO [g]	KH_2PO_4 [g]		[Al, mmol/L]	[g]		
P1-FA-R	1	0.51	22.72	77.28	100	–	–	51.0	1.2
P1-FA-AlN	1	0.51	22.72	77.28	100	650	11.25	46.1[a]	8.0

[a] The crystallization water of aluminum nitrate nonahydrate is taken into account in the calculation of the w/c ratio.

[b] Final setting of the cement pastes by Vicat needle test.

Appendix B. Decomposition of ^{27}Al MAS NMR spectra from the solid fraction of the suspension with aluminum nitrate (S1-AlN)

Hydration time (h)	Al[IV]								Al[V]				Al[VI]							
	δ (ppm)	FWHM (ppm)	G/L	Pop. (%)	δ (ppm)	FWHM (ppm)	G/L	Pop. (%)	δ (ppm)	FWHM (ppm)	G/L	Pop. (%)	δ (ppm)	FWHM (ppm)	G/L	Pop. (%)	δ (ppm)	FWHM (ppm)	G/L	Pop. (%)
0.17	57.60	8.12	0.58	1.49	48.10	10.90	0.80	10.15	21.50	9.00	1.00	1.17	−4.49	6.31	1.00	23.21	−9.46	8.87	0.50	63.98
0.50	57.50	8.10	0.60	2.19	48.40	10.90	0.80	10.80	21.50	9.00	1.00	1.85	−4.50	6.35	1.00	25.20	−9.35	8.90	0.50	59.97
1.00	57.45	8.10	0.60	1.35	47.71	10.90	0.80	10.77	21.50	9.00	1.00	1.26	−4.57	6.30	1.00	23.28	−9.35	8.90	0.50	63.34
4.83	57.46	8.09	0.57	2.27	48.49	10.89	0.78	11.54	21.50	9.00	1.00	1.75	−4.35	6.35	1.00	25.44	−9.30	9.00	0.50	59.00
5.50	57.40	8.10	0.60	1.49	48.10	10.80	0.80	11.70	21.50	9.00	1.00	1.23	−4.50	6.30	1.00	26.90	−9.40	8.90	0.55	58.68
6.00	57.45	8.10	0.60	1.56	48.50	10.90	0.80	11.72	21.50	9.00	1.00	1.50	−4.45	6.42	1.00	28.03	−9.40	8.90	0.50	57.19
24.00	57.40	8.10	0.60	3.31	48.40	10.90	0.80	10.83	21.60	9.00	1.00	2.35	−4.20	6.52	1.00	29.40	−9.40	8.90	0.55	54.11

References

[1] A.S. Wagh, Chemically Bonded Phosphate Ceramics, Elsevier, 2004.

[2] F. Qiao, C.K. Chau, Z. Li, Property evaluation of magnesium phosphate cement mortar as patch repair material, Construct. Build Mater. 24 (2010) 695–700.

[3] B. Xu, F. Winnefeld, J. Kaufmann, B. Lothenbach, Influence of magnesium-to-phosphate ratio and water-to-cement ratio on hydration and properties of magnesium potassium phosphate cements, Cem. Concr. Res. 123 (2019), 105781.

[4] B. Xu, H. Ma, H. Shao, Z. Li, B. Lothenbach, Influence of fly ash on compressive strength and micro-characteristics of magnesium potassium phosphate cement mortars, Cem. Concr. Res. 99 (2017) 86–94.

[5] F. Qiao, C.K. Chau, Z. Li, Setting and strength development of magnesium phosphate cement paste, Adv. Cem. Res. 21 (2009) 175–180.

[6] J. Qin, J. Qian, C. You, Y. Fan, Z. Li, H. Wang, Bond behavior and interfacial micro-characteristics of magnesium phosphate cement onto old concrete substrate, Construct. Build Mater. 167 (2018) 166–176.

[7] H. Lahalle, C. Cau Dit Coumes, A. Mesbah, D. Lambertin, C. Cannes, S. Delpech, S. Gauffinet, Investigation of magnesium phosphate cement hydration in diluted suspension and its retardation by boric acid, Cem. Concr. Res. 87 (2016) 77–86.

[8] H. Lahalle, C.t Cau Dit Coumes, C. Mercier, D. Lambertin, C. Cannes, S. Delpech, S. Gauffinet, Influence of the w/c ratio on the hydration process of a magnesium phosphate cement and on its retardation by boric acid, Cem. Concr. Res. 109 (2018) 159–174.

[9] I. Buj, J. Torras, D. Casellas, M. Rovira, J. de Pablo, Effect of heavy metals and water content on the strength of magnesium phosphate cements, J. Hazard. Mater. 170 (2009) 345–350.

[10] I. Buj, J. Torras, M. Rovira, J. de Pablo, Leaching behaviour of magnesium phosphate cements containing high quantities of heavy metals, J. Hazard. Mater. 175 (2010) 789–794.

[11] Z. Zhang, Z. Yang, Z. Chen, T. Kang, X. Ding, Y. Li, Y. Liao, C. Chen, H. Yuan, H. Peng, J. Lim, A study on bone cement containing magnesium potassium phosphate for bone repair, Cogent Biol. 4 (2018).

[12] Y. Yu, C. Xu, H. Dai, Preparation and characterization of a degradable magnesium phosphate bone cement, Regen. Biomater. 3 (2016) 231–237.

[13] H. Lahalle, C. Patapy, M. Glid, G. Renaudin, M. Cyr, Microstructural evolution/durability of magnesium phosphate cement paste over time in neutral and basic environments, Cem. Concr. Res. 122 (2019) 42–58.

[14] L.J. Gardner, S.A. Bernal, S.A. Walling, C.L. Corkhill, J.L. Provis, N.C. Hyatt, Characterisation of magnesium potassium phosphate cements blended with fly ash and ground granulated blast furnace slag, Cem. Concr. Res. 74 (2015) 78–87.

[15] L.J. Gardner, V. Lejeune, C.L. Corkhill, S.A. Bernal, J.L. Provis, M.C. Stennett, N. C. Hyatt, Evolution of phase assemblage of blended magnesium potassium phosphate cement binders at 200° and 1000 °C, Adv. Appl. Ceram. 114 (2015) 386–392.

[16] Z.H. Qian, X.Y. Liu, Y.B. Qiao, S. Wang, Q. Qin, L.Q. Shi, H.H. Peng, Effect of fluorine on stabilization/solidification of radioactive fluoride liquid waste in magnesium potassium phosphate cement, J. Radioanal. Nucl. Chem. 319 (2018) 393–399.

[17] A. Covill, N.C. Hyatt, J. Hill, N.C. Collier, Development of magnesium phosphate cements for encapsulation of radioactive waste, Adv. Appl. Ceram. 110 (2013) 151–156.

[18] W. Hao, H. Ma, G. Sun, Z. Li, Magnesia phosphate cement composite bipolar plates for passive type direct methanol fuel cells, Energy 168 (2019) 80–87.

[19] Y. Weng, S. Ruan, M. Li, L. Mo, C. Unluer, M.J. Tan, S. Qian, Feasibility study on sustainable magnesium potassium phosphate cement paste for 3D printing, Construct. Build Mater. 221 (2019) 595–603.

[20] H. Ma, B. Xu, J. Liu, H. Pei, Z. Li, Effects of water content, magnesia-to-phosphate molar ratio and age on pore structure, strength and permeability of magnesium potassium phosphate cement paste, Mater. Des. 64 (2014) 497–502.

[21] B. Xu, H. Ma, Z. Li, Influence of magnesia-to-phosphate molar ratio on microstructures, mechanical properties and thermal conductivity of magnesium potassium phosphate cement paste with large water-to-solid ratio, Cem. Concr. Res. 68 (2015) 1–9.

[22] B. Xu, B. Lothenbach, A. Leemann, F. Winnefeld, Reaction mechanism of magnesium potassium phosphate cement with high magnesium-to-phosphate ratio, Cem. Concr. Res. 108 (2018) 140–151.

[23] B. Xu, B. Lothenbach, H. Ma, Properties of fly ash blended magnesium potassium phosphate mortars: effect of the ratio between fly ash and magnesia, Cem. Concr. Compos. 90 (2018) 169–177.

[24] L. Mo, L. Lv, M. Deng, J. Qian, Influence of fly ash and metakaolin on the microstructure and compressive strength of magnesium potassium phosphate cement paste, Cem. Concr. Res. 111 (2018) 116–129.
[25] B. Xu, B. Lothenbach, F. Winnefeld, Influence of wollastonite on hydration and properties of magnesium potassium phosphate cements, Cem. Concr. Res. 131 (2020), 106012.
[26] F. Qiao, C.K. Chau, Z. Li, Calorimetric study of magnesium potassium phosphate cement, Mater. Struct. 45 (2011) 447–456.
[27] S.A. Walling, J.L. Provis, Magnesia-based cements: a journey of 150 years, and cements for the future? Chem. Rev. 116 (2016) 4170–4204.
[28] C. Langton, D. Stefanko, Magnesium mono potassium phosphate grout for p-reactor vessel in-situ decomissioning, United States, 2011.
[29] Y. Li, T. Shi, B. Chen, Experimental sudy of dipotassium hydrogen phosphate influencing properties of magnesium phosphate cement, J. Mater. Civ. Eng. 28 (2016).
[30] C. Qian, J. Yang, Effect of disodium hydrogen phosphate on hydration and hardening of magnesium potassium phosphate cement, J. Mater. Civ. Eng. 23 (2011) 1405–1411.
[31] S. Zhao, H. Yan, H. Zhang, H. Wang, Y. Li, Z. Hu, H. Sun, The effects of admixtures of inorganic hydrates on the hydration hardening of magnesium potassium phosphate cement, Adv. Cem. Res. 30 (2018) 83–92.
[32] R. Boncukcuoğlu, M.T. Yılmaz, M.M. Kocakerim, V. Tosunoğlu, Utilization of borogypsum as set retarder in Portland cement production, Cem. Concr. Res. 32 (2002) 471–475.
[33] S.Y. Oderji, B. Chen, C. Shakya, M.R. Ahmad, S.F.A. Shah, Influence of superplasticizers and retarders on the workability and strength of one-part alkali-activated fly ash/slag binders cured at room temperature, Construct. Build Mater. 229 (2019), 116891.
[34] J.-B. Champenois, M. Dhoury, C. Cau Dit Coumes, C. Mercier, B. Revel, P. Le Bescop, D. Damidot, Influence of sodium borate on the early age hydration of calcium sulfoaluminate cement, Cem. Concr. Res. 70 (2015) 83–93.
[35] C. Cau Dit Coumes, M. Dhoury, J.-B. Champenois, C. Mercier, D. Damidot, Combined effects of lithium and borate ions on the hydration of calcium sulfoaluminate cement, Cem. Concr. Res. 97 (2017) 50–60.
[36] C. Cau Dit Coumes, D. Lambertin, H. Lahalle, P. Antonucci, C. Cannes, S. Delpech, Selection of a mineral binder with potentialities for the stabilization/solidification of aluminum metal, J. Nucl. Mater. 453 (2014) 31–40.
[37] S. Delpech, C. Cannes, N. Barré, Q.T. Tran, C. Sanchez, H. Lahalle, D. Lambertin, S. Gauffinet, C. Cau Dit Coumes, Kinetic model of aluminum behavior in cement-based matrices analyzed by impedance spectroscopy, J. Electrochem. Soc. 164 (2017) C717–C727.
[38] C.K. Chau, F. Qiao, Z. Li, Potentiometric study of the formation of magnesium potassium phosphate Hexahydrate, J. Mater. Civ. Eng. 24 (2012) 586–591.
[39] P.K. Mehta, D. Pirtz, Magnesium oxide additive for producing self-stress in mass concrete, in: Proc 7th Intern. Congress on the Chemistry of Cement, Paris, France, 1980.
[40] J. Van Der Lee, Thermodynamic and Mathematical Concepts of CHESS, T.R, 1998. LHM/RD/98/39.
[41] B. Lothenbach, B. Xu, F. Winnefeld, Thermodynamic data for magnesium (potassium) phosphates, Appl. Geochem. 111 (2019), 104450.
[42] P. Blanc, A. Lassin, P. Piantone, M. Azaroual, N. Jacquemet, A. Fabbri, E. C. Gaucher, Thermoddem: a geochemical database focused on low temperature water/rock interactions and waste materials, Appl. Geochem. 27 (2012) 2107–2116.
[43] Lawrence Livermore National Laboratory (LLNL) database, provided with Chess software.
[44] T.Y. Vieillard, Thermochemical properties of phosphates, in: M.P.B.e, in: J. O. Nriagu (Ed.), Phosphate Minerals, Springer, Berlin, Heidelberg, 1984.
[45] J.A. Veith, G. Sposito, Reactions of Aluminosilicates, aluminum hydrous oxides, and aluminum oxide with o-phosphate: the formation of X-ray amorphous analogs of variscite and montebrasite, J. Soil Sci. 41 (1977) 870–876.
[46] A.W. Taylor, E.L. Gurney, Solubilities of potassium and ammonium taranakites, J. Phys. Chem. 65 (1961) 1613–1616.
[47] A. Samadi-Maybodi, S.K.H. Nejad-Darzi, H. Bijanzadeh, ^{31}P and ^{27}Al NMR studies of aqueous (2-hydroxyethyl) trimethylammonium solutions containing aluminum and phosphorus, Spectrochim. Acta A Mol. Biomol. Spectrosc. 72 (2009) 382–389.
[48] R. Lookman, P. Grobet, R. Merckx, K. Vlassak, Phosphate sorption by synthetic amorphous aluminium hydroxides: a ^{27}Al and ^{31}P solid-state MAS NMR spectroscopy study, Eur. J. Soil Sci. 45 (1994) 37–44.
[49] K.J.D. MacKenzie, M.E. Smith, Multinuclear Solid-State NMR of Inorganice Materials, Pergamon, in: Materials Series, Elsevier, Oxford UK, 2002, pp. 438–452.
[50] C. Martineau, B. Bouchevreau, Z. Tian, S.-J. Lohmeier, P. Behrens, F. Taulelle, Beyond the limits of X-ray powder diffraction: description of the nonperiodic subnetworks in aluminophosphate-cloverite by NMR crystallography, Chem. Mater. 23 (2011) 4799–4809.
[51] L. van Wüllen, S. Wegner, G. Tricot, Structural changes above the glass transition and crystallization in aluminophosphate glasses: an in situ high-temperature MAS NMR study, J. Phys. Chem. B 111 (2007) 7529–7534.
[52] M. Haouas, C. Martineau, F. Taulelle, Quadrupolar NMR of nanoporous materials, in: R.K. Harris, R.L. Wasylishen (Eds.), eMagRes, John Wiley and Sons, Hoboken, New Jersey, US, 2011.
[53] J.O. Nriagu, Phosphate – clay mineral relations in soils and sediments, Can. J. Earth Sci. 13 (1976) 717–736.
[54] U.G.A. Weiss, Ch. Roble, Transformation of clay minerals into taranakite and the crystal structure of taranakite, in: R.W.F.G.T. Churchman, R.A. Eggleton (Eds.), Clays, Controlling the Environment, Proc. 10th Int, Clay Conf. Adelaïde, Australia, 1993, p. 253.
[55] J.F. Haseman, E.H. Brown, C.D. Whitt, Some reactions of phosphate with clays and hydrous oxides of iron and aluminum, Soil Sci. 70 (1950) 257–272.
[56] S. Dick, U. Goβner, A. Weiβ, C. Robl, G. Groβmann, G. Ohms, T. Zeiske, Taranakite — the mineral with the longest crystallographic axis, Inorg, Chim. Acta 269 (1998) 47–57.
[57] T.Z.S. Dick, Francoanellite $K_3Al_5(HPO_4)_6(PO_4)_2{\cdot}12H_2O$: structure and synthesis by topochemical dehydration of taranakite, Z. Naturforsch., B: J. Chem. Sci. 53 (1998) 711–719.
[58] J.F. Haseman, J.R. Lehr, J.P. Smith, Mineralogical character of some iron and aluminum phosphates containing potassium and ammonium, Soil Sci. 15 (1951) 76–84.
[59] A.R. Kampf, Minyulite; its atomic arrangement, Am. Mineral. 62 (1977) 256–262.
[60] S. Dick, G. Grossmann, G. Ohms, T. Zeiske, Aluminum phosphates with non-centrosymmetric layer- and framework-structures of topologically related motifs. Part 1. $KAl_2(PO_4)_2(OH){\cdot}4H_2O$, Z. Naturforsch., B: J. Chem. Sci. 52 (1997) 1439–1446.
[61] S. Dick, The structure of synthetic tinsleyite $K[A1_2(PO_4)_2(OH){\cdot}2H_2O]$|Uber die Struktur von synthetischen Tinsleyit $KAl_2(PO_4)_2(OH){\cdot}2H_2O$, Z. Naturforsch. 54 b (1999) 1385–1390.
[62] S. Dick, G. Grossmann, G. Ohms, M. Mueller, Aluminum phosphates with non-centrosymmetric layer- and framework-structures of topologically related motifs: 2. $KAl_2(PO_4)_2(OH){\cdot}2H_2O$|Aluminiumphosphate mit nichtzentrosymmetrischen schicht- und raumnetzstrukturen aus topologisch verwandten motiven: 2. $KAl_2(PO_4)_2(OH){\cdot}2H_2O$, Z. Naturforsch., B: J. Chem. Sci. 52 (1997) 1447–1455.
[63] S. Dick, U. Goßner, A. Weiss, C. Robl, G. Grossmann, G. Ohms, M. Müller, The potassium aluminum phosphate $KAl(HPO_4)_2{\cdot}H_2O$: X-ray diffraction, neutron-scattering, and solid-state NMR characterization, J. Solid State Chem. 132 (1997) 47–55.
[64] J. Klein, M. Ushio, L.S. Burrell, B. Wenslow, S.L. Hem, Analysis of aluminum hydroxyphosphate vaccine adjuvants by ^{27}Al MAS NMR, J. Pharm. Sci. 89 (2000) 311–321.
[65] R. Lookman, P. Grobet, R. Merckx, W.H. Van Riemsdijk, Application of ^{31}P and ^{27}Al MAS NMR for phosphate speciation studies in soil and aluminium hydroxides: promises and constraints, Geoderma 80 (1997) 369–388.
[66] T. Isobe, T. Watanabe, J.B. d'Espinose de la Caillerie, A.P. Legrand, D. Massiot, Solid-state ^{1}H and ^{27}Al NMR studies of amorphous aluminum hydroxides, J. Colloid Interface Sci. 261 (2003) 320–324.
[67] A.C. Kunwar, A.R. Thompson, H.S. Gutowsky, E. Oldfield, Solid state aluminum-27 NMR studies of tridecameric Al-oxohydroxy clusters in basic aluminum selenate, sulfate, and the mineral zunyite, J. Magn. Reson. 60 (1984) 467–472.
[68] S.J. Duffy, G.W. Van Loon, Investigations of aluminum hydroxyphosphates and activated sludge by ^{27}Al and ^{31}P MAS NMR, Can. J. Chem. 73 (1995) 1645–1659.
[69] D. Müller, I. Grunze, E. Hallas, G. Ladwig, Hochfeld-27Al-NMR-Untersuchungen zur Aluminiumkoordination in kristallinen Aluminiumphosphaten, Z. Anorg. Allg. Chem. 500 (1983) 80–88.
[70] T.T.P. Cheung, K.W. Willcox, M.P. McDaniel, M.M. Johnson, C. Bronnimann, J. Frye, The structure of coprecipitated aluminophosphate catalyst supports, J. Catal. 102 (1986) 10–20.
[71] C.S. Blackwell, R.L. Patton, Aluminum-27 and phosphorus-31 nuclear magnetic resonance studies of aluminophosphate molecular sieves, J. Phys. Chem. 88 (1984) 6135–6139.
[72] W.F. Bleam, P.E. Pfeffer, J.S. Frye, ^{31}P solid-state nuclear magnetic resonance spectroscopy of aluminum phosphate minerals, Phys. Chem. Miner. 16 (1989) 455–464.
[73] Z.R. Hinedi, A.C. Chang, J.P. Yesinowski, Phosphorus-31 magic angle spinning nuclear magnetic resonance of wastewater sludges and sludge-amended soil, Soil Sci. Soc. Am. J. 53 (1989) 1053–1056.
[74] W.F. Bleam, P.E. Pfeffer, J.S. Frye, ^{31}P and ^{27}Al solid-state nuclear magnetic resonance study of taranakite, Phys. Chem. Miner. 16 (1989) 809–816.
[75] E. Dumas, F. Taulelle, G. Férey, Synthesis and crystal structure of the synthetic analogue of mineral minyulite $K[Al_2F(H_2O)_4(PO_4)_2]$, Solid State Sci. 3 (2001) 613–621.